A low-density ocean inside Titan inferred from Cassini data

Goossens, Sander; van Noort, Bob; Mateo, Alfonso; Mazarico, Erwan; van der Wal, Wouter

DOI
10.1038/s41550-024-02253-4

Publication date
2024

Document Version
Final published version

Published in
Nature Astronomy

nature astronomy

Article

https://doi.org/10.1038/s41550-024-02253-4

A low-density ocean inside Titan inferred from Cassini data

Received: 20 April 2023

Accepted: 21 March 2024

Published online: 29 April 2024

Check for updates

Sander Goossens[1] ✉, Bob van Noort[2,3,4,5], Alfonso Mateo[4,6], Erwan Mazarico[1] & Wouter van der Wal[4]

The Cassini mission has provided measurements of the gravity of several moons of Saturn as well as an estimate of the tidal response, which is expressed as the degree 2 Love number k_2 of its largest moon, Titan. The first estimates of Titan's Love number were larger than pre-Cassini expectations. Interior modelling suggested it may be explained with a dense ocean, but the interpretation remains unclear. We analysed Cassini tracking data to determine Titan's gravity field and its Love number. Our gravity results are consistent with earlier studies, but we find a lower Love number for Titan of $k_2 = 0.375 \pm 0.06$. This lower value follows from an elaborate investigation of the tidal effects. We show that a dense ocean is not implied by the obtained Love number; instead, a water or ammonia ocean is more probable. A lower density ocean can increase the likeliness of contact between the silicate core and ocean, which can leach minerals into the ocean and could promote its habitability.

The Cassini mission explored Saturn and its icy moons for more than a decade. Among its many instruments, Cassini carried a radio science subsystem that enabled Earth-based radiometric tracking of the spacecraft by the Deep Space Network. These data were used to determine the gravity field and interior structure of several of Saturn's moons[1–4] as well as those of Saturn itself[5]. Cassini data were also used to determine Titan's tidal response[6], expressed as its degree 2 potential Love number k_2. This dimensionless parameter describes how the gravitational field of a self-gravitating body changes in response to forcing by the gravitational field of a disturbing body, which in this case is Saturn.

To explain the presence of methane on the surface of Titan, thermal modelling of its interior predicted that it could contain an internal ocean[7]. Additional modelling suggested that an ammonia-rich liquid layer may be present under an icy shell[8–10] and that Cassini may be able to detect such a subsurface ocean from measurements of Titan's Love number[11,12]. Knowledge of the composition of the ocean, as expressed, for example, in its density, is important as it influences melting curves and interior temperature profiles. This in turn influences the interior layering and possible contact between the ocean and its silicate core, which has implications for habitability[10,13,14].

Initially, Titan's gravity field, without k_2, was estimated up to spherical harmonic degree and order 3 from four fly-bys[1]. Adding two more fly-bys allowed k_2 to be estimated, resulting in values of $k_2 = 0.589 \pm 0.15$ and $k_2 = 0.637 \pm 0.224$ using two different processing strategies[6]. These values confirmed the presence of a global ocean. Yet, although a dense ocean could account for the estimated k_2 range (which was larger than expected[10]), a water or ammonia-based ocean with a thin shell (generally considered to be less than 100 km), as favoured by evolution models, is consistent only with the lower end of this k_2 range[6].

Subsequent analyses using refined interior modelling, some with additional data from, for example, Titan's obliquity[15] or shape[16], found that only models with a dense ocean could satisfy the k_2 constraint[17–19]. Models of Titan's interior consistent with the moon's mean density, polar moment of inertia factor and obliquity, were also consistent only with the lower end of the k_2 estimate; it was argued that the higher k_2 value could be matched by a denser ocean or mushy lower ice layers, but their existence was not supported by evidence[13].

[1]NASA Goddard Space Flight Center, Greenbelt, MD, USA. [2]Southeastern Universities Research Association, Washington DC, USA. [3]Center for Research and Exploration in Space Science and Technology (CRESST) II, College Park, MD, USA. [4]Faculty of Aerospace Engineering, Delft University of Technology, Delft, The Netherlands. [5]Present address: Faculty of Civil Engineering and Geosciences, Delft University, Delft, The Netherlands. [6]Present address: Universidad Politécnica de Madrid, Madrid, Spain. ✉e-mail: sander.j.goossens@nasa.gov

https://doi.org/10.1038/s41550-024-02253-4

Analysis of the entire set of ten Titan fly-bys resulted in a Love number $k_2 = 0.616 \pm 0.067$ (ref. 3), close to the earlier results. Interpretation of the Love number remained unclear: the high value could indicate a high-density ocean, a partially viscous response of the deeper regions of the moon or a dynamic contribution to the tidal response, such as non-resonant dynamic tides[3]. An accurate determination of the Love number is, thus, crucial for determining the existence of an ocean and being able to place constraints on its composition.

Results

We have processed Cassini radiometric tracking data with different tools and analysis methods from earlier efforts ('Data analysis' in Methods). We determined gravity field models for Enceladus and Titan, including Titan's Love number. Our solutions for both moons are listed in Supplementary Table 1. We discuss results for Enceladus as validation of our processing.

Enceladus's gravity

Following earlier work[20], we determined a degree and order 2 field for Enceladus, together with the zonal term J_3 (gravity is expressed in spherical harmonics of degree n and order m with coefficients $C_{n,m}$ and $S_{n,m}$, and $J_n = -C_{n,0}$). The terms that are well determined (that is, with relatively small uncertainties) are J_2 and $C_{2,2}$. The zonal term J_3 has a formal error slightly larger than half of the coefficient value. The values of $C_{2,1}$, $S_{2,1}$ and $S_{2,2}$ are relatively large. These coefficients are related to Enceladus's orientation, as they would be zero in a principal axis system. With only three fly-bys, our solutions are not sensitive to these. When we constrain them to be small, the other coefficients are not substantially affected.

We found the ratio $J_2/C_{2,2} = 3.30 \pm 0.27$ (errors are 1σ unless indicated otherwise), which is very close to the hydrostatic equilibrium expectation of 10/3. We used the Darwin–Radau relationship[21] to determine Enceladus's polar moment of inertia factor $C/(MR^2)$, where C is the polar moment of inertia, M the mass and R the radius (252 km). We found that $C/(MR^2) = 0.345 \pm 0.01$, which suggests differentiation of the moon with a rocky core at its centre.

Titan's gravity and tides

For Titan, we estimated values for the full degree and order 5 field and its Love number, similar to earlier work[3]. We show Titan's radial accelerations in Fig. 1. Several of the larger anomalies are below ground tracks, yet the stronger negative gravity anomaly in 60°–120° E and 30°–90° N is not, and it is, thus, much more uncertain, as confirmed by the map of anomaly errors (Supplementary Fig. 1).

We show the power in the gravity field in Fig. 2, together with the power per degree of the formal errors. The power in our solution increases for degrees 4 and 5, compared to degrees 2 and 3. This may be due to gaps in the geographical coverage of the fly-bys (Fig. 1), resulting in not enough resolution to estimate a full degree and order 5 field. This could indicate the need for constraints, but we decided not to apply constraints on the gravity coefficients ('Data analysis' in Methods). The degree 2 and order 1 coefficients are small due to better coverage, which indicates a better sensitivity than we found for Enceladus and agreement with the rotational model we used for Titan in our analysis[22].

As for Enceladus, the J_2 and $C_{2,2}$ coefficients are the coefficients that are determined best. Note that the relative errors for these coefficients are smaller for Enceladus than for Titan, despite having many fewer fly-bys, which is probably due to the larger values of the coefficients. For Titan, we found the ratio $J_2/C_{2,2} = 3.21 \pm 0.72$. This is slightly lower than the hydrostatic ratio but within 1σ. Using the Darwin–Radau relationship, we found a polar moment of inertia ratio $C/(MR^2) = 0.348 \pm 0.03$ (where we used a radius of 2,575 km for Titan). This also indicates that Titan is differentiated. Such a moment of inertia factor can also be consistent with a fully differentiated interior consisting of an icy shell over a low-density core[23].

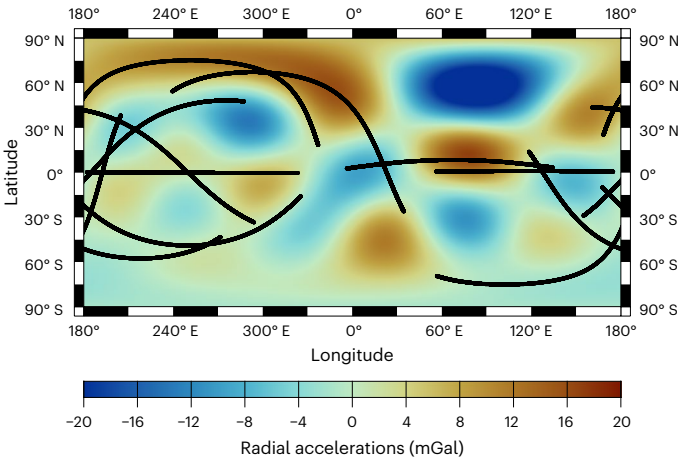

Fig. 1 | Titan's gravity expressed as radial accelerations. The ground tracks of the fly-bys used in the determination of the gravity field model are indicated in black for altitudes less than 9,000 km. We set the coefficients $C_{2,0}$ and $C_{2,2}$ to zero for this map.

Because the $J_2/C_{2,2}$ ratio differs from the hydrostatic value and considering its large uncertainty, non-hydrostatic contributions may be present, which would affect the inertia factor estimate[24] and may also affect the librations[25]. Following earlier analysis[3], we can account for this to some extent by assuming a hydrostatic and non-hydrostatic part for each coefficient. Doing so we can find the hydrostatic part of the total coefficient by minimizing the root mean square (RMS) of the differences between the total and hydrostatic coefficients for both J_2 and $C_{2,2}$, where the hydrostatic parts have direct expressions dependent on the fluid Love number[26], which is the Love number that characterizes the long-term rotational and tidal distortions, in the limit that the exciting period goes to infinity. This results in a slightly higher moment of inertia factor $C/(MR^2) = 0.354 \pm 0.01$ when using the hydrostatic parts of the coefficients.

The tides raised on Titan by Saturn change Titan's degree 2 gravity field, and this effect, modelled with the Love number k_2, can be estimated directly using the response to a tidal potential or through time variations in the degree 2 coefficients; the results of both methods are identical (see Discussion and 'Modelling the tidal effects' in Methods for more details). Fly-bys of Titan dedicated to gravity occurred at different mean anomalies of Titan in its orbit around Saturn (see the fly-by characteristics in Supplementary Table 2), which increases the observability of the tides[3]. We iterated gravity solutions, gradually expanding the maximum spherical harmonic degree ('Data analysis' in Methods). We estimated k_2 for different expansions and based our final result on a series of degree and order 5 fields. We found the mean and standard deviation of all these solutions $k_2 = 0.375 \pm 0.06$, and extreme values of 0.25 and 0.49. The higher values were found with low expansion degrees and when weighting the data uniformly ('Data analysis' in Methods), but the solutions for k_2 are generally in the 0.3–0.4 range. Each separate solution has a formal error close to 0.13; as indicated, our quoted error is from the spread in solutions, which was half the formal error of the individual solutions.

Discussion

Fly-bys have only a limited sensitivity to the gravity field coefficients, due to their limited spatial coverage (Fig. 1 and Supplementary Fig. 1 for Titan and Supplementary Fig. 2 for Enceladus), but at least the J_2 and $C_{2,2}$ terms should be determined well for both moons: these terms are by far the largest (due to rotational and tidal forces), and the ground track coverage for the moons is such that both terms should be determined well (there are high- and low-inclination tracks). For both Enceladus

https://doi.org/10.1038/s41550-024-02253-4

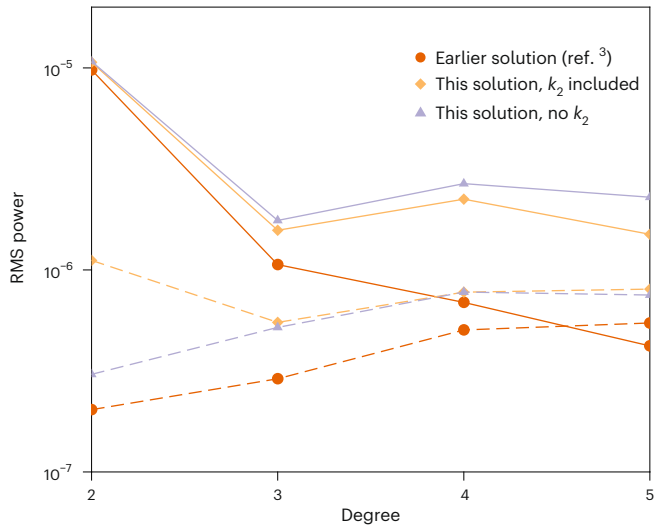

Fig. 2 | RMS power for Titan's gravity. We show the RMS power for our solution and an earlier solution[3]. The coefficients were normalized following standard geodesy conventions[47]. The dashed lines indicate the RMS power for the formal errors.

and Titan, we found good agreement with earlier analyses[1,3,20] for these coefficients. For Enceladus, our J_2 is slightly smaller and $C_{2,2}$ is slightly higher, resulting in a smaller $J_2/C_{2,2}$ ratio, but the ratio is consistent within 1σ. Our J_3 term is larger (in an absolute sense), but it also has a relatively large error. For Titan, our $J_2/C_{2,2}$ ratio is very close to that from earlier analyses[1,3], whereas our individual coefficients are slightly different (see Supplementary Table 1 for a comparison with earlier results). They are generally consistent within 1σ and, thus, not significantly different. These results, together with good levels of fit to the data (the close-approach signal in the tracking data residuals disappears after gravity estimation; see 'Data analysis' in Methods), indicate the validity of our processing and provide confidence in our solutions.

Our reported errors are higher than those from earlier results using the same data. This may partly be because we used 10 s of data instead of 60 s: shorter count intervals in general increase the intrinsic noise although thermal noise is deemed minor for Cassini[27]. We also used a different data weighting scheme, and we applied variance component estimation (VCE) in our estimation, where each fly-by is a statistical set for which a weight factor is determined ('Data analysis' in Methods). The formal errors from our solutions were, thus, calibrated such that the formal statistics match the observed statistics (variations in the data residuals from cyclically randomizing the statistical sets), resulting in higher formal errors for the gravity coefficients (Fig. 2). The error for degree 2 was larger when we estimated k_2. This was due to correlations between k_2 and the degree 2 gravity terms ('Modelling the tidal effects' in Methods).

As stated earlier, the power in the degree 4 and 5 terms of Titan's field is larger than that of earlier analysis[3], which found the spectrum to follow a power law (Kaula rule) of $10^{-5}/n^2$ (with n the spherical harmonic degree). The higher-degree expansions did not significantly affect the lower-degree coefficients; our k_2 estimate was only slightly affected. We noticed that the fit to the data did not improve much when we estimated a degree and order 4 or 5 field compared to a degree and order 3 field (Supplementary Fig. 3), which indicates that the solutions are probably not sensitive to a full 5 by 5 field. We estimated the full degree and order 5 field nonetheless to prevent possible aliasing of an additional signal into the lower-degree terms. We did not constrain the gravity parameters to follow a Kaula rule as the knowledge of the gravity fields of icy bodies is currently too limited to make definite statements about the expected power spectrum[28]. The higher-degree terms were not determined well; for several, the formal error was larger than the coefficient value, which was also noted in earlier work[3].

Having established that the solutions agree for the important degree 2 terms, we next investigated differences with the earlier studies in the estimate of k_2. As indicated, our analysis can account for the effects of the tides in two separate ways: through a direct tidal potential or through the time-varying effects on degree 2 coefficients ('Modelling the tidal effects' in Methods). We used both tidal models separately in our processing, which resulted in the same estimated k_2 value.

Earlier work[6] considered the time-varying effects on the degree 2 terms. Note, however, that there are three core differences with how the tides are accounted for, compared to our analysis. First, an approximated tidal potential[11,12] was used, whereas we used a more general expression that does not rely on assumptions about Titan's orbit[29,30]. Second, we note a discrepancy of a factor of 2 in the time-dependent k_2 contribution to the $S_{2,2}$ term, which makes the term smaller compared to the cited pre-Cassini work[11,12] that their expressions are based on. Third, the time-varying effects of k_2 on the degree 2 terms are not correctly accounted for in the partial derivatives; these relate changes in the data residuals to changes in the k_2 parameter and are critical for forming linearized observation equations and estimating the parameter.

Because the effects of k_2 on the degree 2 terms are time-dependent, they should be accounted for by combining them with the partials for the degree 2 gravity terms in the numerical integration of the variational equations. However, in the earlier analysis of Cassini data[6], they were combined with the degree 2 terms after the variational equations were integrated. We show that this results in an observation equation system that does not correctly relate changes in the estimated parameters with changes in the data residuals ('Estimating k_2' in Methods).

When we altered our own estimation scheme to follow the earlier analysis, we could replicate their results; we then also obtained larger Love numbers (Supplementary Table 3). The first difference is probably of little consequence as the approximated tidal potential is close to the more general one ('Modelling the tidal effects' in Methods). The discrepancy in the $S_{2,2}$ factor by itself should also in principle not influence the results too much, because the J_2 and $C_{2,2}$ effects on k_2 are much larger (see the discussion on the permanent contributions to the degree 2 terms in 'Modelling the tidal effects' in Methods). However, constructing the partials from which k_2 is estimated without taking into account the effect of k_2 on the degree 2 terms during the numerical integration of the variational equations compounds with the other two differences and results in an overestimation of k_2.

We could reproduce the earlier results with the incorrect partials. A later solution[3] may have used the correct partials (private communication), yet this is not documented. Those authors found results very consistent with the earlier ones ($k_2 = 0.616$), which is surprising, as we found that the partials had a strong influence on the resulting value, and thus, we would expect at least a change in the k_2 value when using different tidal modelling. We could not reproduce the later results when using the correct partials. Also, we could not explain the differences in k_2 as due to the use of constraints or a different maximum degree and order of the expansion. When we used the later results[3] as a starting point in our analysis, including k_2, we still found a lower Love number. Our results never reached high k_2 values; we, therefore, conclude that the application of the correct partials leads to a Love number estimate that is robustly in the range 0.3 to 0.4.

Analyses of interior models for Titan based on the higher Love number found a need for a dense ocean to match the Love number constraint, which often was still only satisfied at the lower end of its uncertainty. Our lower value is closer to pre-Cassini predictions[10]. Together with our estimate for Titan's moment of inertia and its bulk density (obtained from the value of GM; see Supplementary Table 1), we can use the Love number to determine the parameters for an interior structure model of Titan to probe whether a dense ocean is still implied.

https://doi.org/10.1038/s41550-024-02253-4

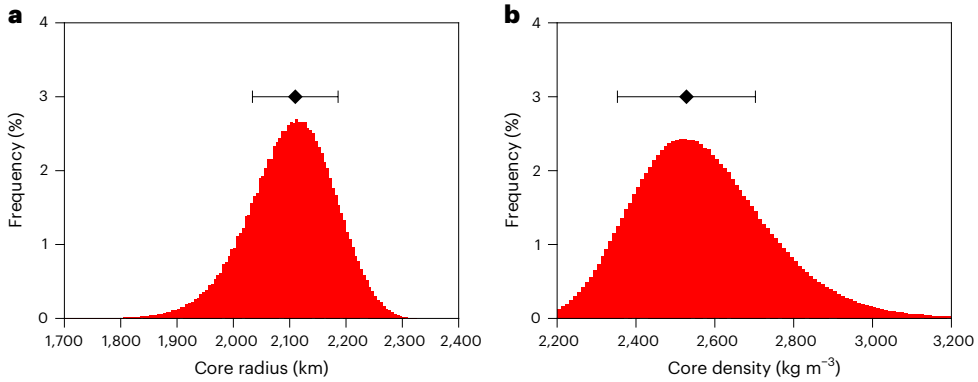

Fig. 3 | Properties of Titan's core. a,**b**, A posteriori distributions (including the central value ± 1 standard deviation) of the core radius (**a**) and core density (**b**) for Titan as the results from our MCMC analysis to match the moment of inertia, bulk density and Love number. We evaluated 500,000 models with 40 chains.

For completeness, we also include Enceladus in our analysis but we discuss the results only in 'Interior modelling' (Methods).

We modelled Titan's interior as a spherically symmetric body. We assumed four layers: a rocky core, a high-pressure ice shell, an ocean and an icy crust[14,17,31], with a fixed total radius of 2,575 km. Based on a recent analysis[31], we computed realistic density profiles for the hydrosphere for various ocean compositions (pure water and various weight percentages of $MgSO_4$) and temperatures at the bottom of the ice shell (which is a proxy for the shell thickness), and compared the tidal response of such profiles to that of a model with layers of constant density (where the constant density was the average of the density profile in each layer; all other parameters, which are discussed below, were kept the same). We show such a density profile in Supplementary Fig. 4. We found that accounting for the increase of density with depth increases the Love number by at most 4%, which is smaller than the current error on k_2 and in agreement with earlier results[17].

Given the large impact of the ocean density on the predicted Love number[14,17,31] and the significantly lower Love number, we found it more prudent to use a simplified model with parameters that previous analyses have shown to have the most influence on k_2. We, thus, used a model with constant densities in our subsequent analysis.

We varied the core radius and density, ocean thickness and density (the ice shell thickness was also varied; it was determined automatically from the fixed planet radius and other radii values), and the viscosity of the high-pressure ice and icy crust, within given limits ('Interior modelling' in Methods and Supplementary Table 4 for values and their ranges). We explored the parameter space using a Markov chain Monte Carlo (MCMC) approach[32] to match the moment of inertia factor (we used our value of $C/(MR^2) = 0.348 \pm 0.03$), bulk density and Love number. To compute Titan's tidal response, we used a Maxwell rheology for Titan but found that we obtained the same results with an Andrade rheology.

We found that the moment of inertia factor is mostly sensitive to the core parameters. The error on the polar moment of inertia factor is such that we could not determine the ocean thickness or icy crust thickness with certainty. We generally found solutions close to our minimum ocean thickness (50 km) but thicker oceans were also possible. We show histograms for the core radius and density in Fig. 3 and distributions for all parameters and measurements in Supplementary Fig. 5, which allows for additional considerations of the sensitivity of our results. We found a core size of 2,110 ± 76 km and a core density of 2,528 ± 175 kg m^{-3} from the modes of the distributions. Both values are consistent with models from a recent review of Titan's interior[14].

We show the relationship between ocean density and k_2 in Fig. 4 as a heat map of model counts from our results. Our analysis clearly favours lower densities for Titan's ocean. We obtained an ocean density of 1,091 ± 107 kg m^{-3} as the mean and standard deviation of the

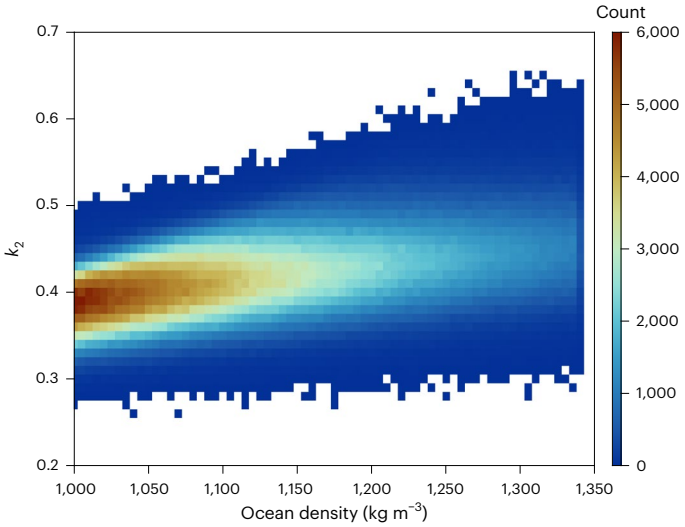

Fig. 4 | Ocean density versus Love number k_2 for Titan. The results are displayed as a heat map using the counts from our MCMC analysis.

distribution of ocean densities. Larger densities are less probable, and indeed, result in larger Love numbers. A dense ocean is, thus, not implied from matching our estimate of Titan's Love number.

We tested a wide range of viscosities and rigidities for the layers pertinent to the tidal response, and the results showed only low sensitivities, like those of an earlier study[17]. Our simplified modelling may have resulted in weaker sensitivities with respect to the viscosities and rigidities compared to more complete models with temperature-dependent viscosity profiles. Such models would include viscosity changes with depth, which would affect the tidal response. Still, studies that have applied more complete models all indicated that a lower Love number is correlated with lower ocean densities[13,17,31].

The density of an ocean depends on its composition[31]. The density also affects the thickness of the crust and the high-pressure ice layer through its effect on temperature profiles[14]. A thin icy crust and a less dense ocean may result in a thin or even absent high-pressure layer. This in turn would make contact between the ocean and core more probable and increase the chance that volatiles and organics in the core could be transported into the ocean with implications for astrobiology[14]. Previous analyses of Titan's interior using the higher Love number focused on increasing the ocean density by looking at different compositions. An ocean with a higher weight percentage of $MgSO_4$ has a higher density compared to pure water or an ocean with NH_3 (ref. 31); our lower Love number implies a lower density, which favours water or NH_3 oceans.

Our results, thus, have important implications for our knowledge of Titan's interior structure, ocean composition and potential habitability.

Methods

Data analysis

We processed radiometric X-band tracking data from the Deep Space Network in continuous spans of time called 'arcs' using the GEODYN II software produced by NASA's Goddard Space Flight Center (GSFC)[33]. We did not include data with an X band for the uplink or with a Ka band for the downlink; the Sun-Earth-Probe angles[3] are such that plasma effects are likely small. We numerically integrated the equations of motion for both the central body (Enceladus or Titan) and the spacecraft, using high-fidelity models for the forces. The forces on the spacecraft include the following: the central body's gravity field (and tides, for Titan); third-body perturbations by Saturn, its seven largest moons (Iapetus, Dione, Enceladus or Titan, Mimas, Tethys, Rhea and Hyperion), and the Solar System bodies (including the Moon and Pluto); Saturn's gravity (its zonal harmonics) and its rings[5]; solar radiation and drag (we include a model of Cassini's shape in our analysis); and accelerations induced by the radioisotope thermoelectric generators (RTGs). For the RTG accelerations, we use the model applied to Cassini by earlier analysis, taking into account the half-life of plutonium[1,34]. For the central bodies, the forces consist of the gravitational forces of the other bodies. We used rotational elements for Enceladus as recommended by the International Astronomical Union[35]. For Titan, we used those from Cassini results[22]. For the positions of the moons and bodies as well as the initial position and velocity of Cassini, we used values from a reconstructed trajectory[36], which were based on JPL planetary ephemeris DE435 and Saturn satellite ephemeris SAT409.

We modelled the measurements using highly accurate and state-of-the art models, including but not limited to effects from the troposphere and ionosphere and effects from ocean loading on the Deep Space Network sites. All fly-bys used the high-gain antenna except for T110, which used the low-gain antenna. We modelled the positions of each. We clearly saw a signal due to antenna motion in T110 when we did not use updated low-gain antenna coordinates[37].

We divided the set of estimated parameters into two groups: local parameters that only affect measurements in one arc and global parameters that affect measurements for all arcs. The local parameters are the following: the state (position and velocity) at the initial epoch for both the spacecraft and central body, a scaling coefficient for solar radiation pressure, scaling coefficients in the spacecraft frame for the RTG accelerations, and a measurement bias for three-way Doppler data (different transmitting and receiving stations) to account for differences in reference frequency at the stations. We used three-way data only if they were collected during closest approach; they were then used in addition to two-way data, just because this is the most important time span of the data collection. We also estimated a drag scaling coefficient for each Titan fly-by and velocity adjustments at closest approach for two of the three Enceladus fly-bys to account for the effects of plumes[20]. The global parameters are the coefficients of a spherical harmonic expansion of the gravity field, the body's gravitational parameter GM and, for Titan, its Love number k_2.

For the ten fly-bys dedicated to Titan gravity, we processed the data in arcs with an average length of slightly more than 2 days, excluding spacecraft manoeuvres, thruster firings or angular momentum desaturation events that could impart residual accelerations on the spacecraft. For Enceladus, there were three fly-bys dedicated to gravity. We processed these data in arcs with lengths slightly over 1 day. For each arc, we processed the data to adjust the local parameters. We compared the modelled measurements with the actual observations (their differences are the residuals) and adjusted the local parameters in a batch least-squares sense[38,39]. An arc was considered to have converged when changes in the RMS of the residuals were 1% or less. We then generated partial derivatives of the measurements with respect to all parameters and formed the normal equation system. The normal equations from all fly-bys for one body were then combined, with weights per fly-by being determined using VCE (see below)[40]. We repeated this entire process (estimating the local and global parameters) several times until the results were deemed to have converged (see below).

We used data averaged over 10 s for the fly-bys of both bodies. We weighted the data uniformly at 28 mHz during the determination of the local parameters, corresponding to 0.5 mm s^{-1} for X-band data. Because we used 10 s of data, our RMS values for the fits are generally a little higher than those for earlier analysis[3], which used 60 s of data. We show an example of data residuals before and after gravity estimation in Supplementary Fig. 6. The closest-approach signal is clearly visible in the residuals before gravity estimation. After gravity adjustment, the residuals resemble data noise. When we used 60 s of data, the fit improved at a level commensurate with the longer count interval, as expected. We have no indication that the higher intrinsic noise level of 10 s data affected our results; as mentioned, thermal noise was deemed to be minor for Cassini[27]. We selected the shorter count interval to ensure we had a good sampling of the gravity field. At Titan (with fly-by speeds around 6 km s^{-1} with respect to the moon), this was not an issue due to its large size, but at Enceladus (at fly-by speeds between 6.5 and 7.5 km s^{-1}), a degree 2 field would run the risk of being undersampled if we used 60 s of data. We show the RMS of the data fit in Supplementary Fig. 7. It was clearly fitted well below the data weight of 28 mHz. When we used the gravity model from earlier Cassini analysis[3] for our Titan analysis, we obtained similar fits as with our own model.

We applied constraints during the determination of the local and global parameters, but mostly they were weak. Generally the parameters were adjusted at levels well below their constraint. We left Cassini's state (position and velocity) unconstrained. The central body's state during the determination of the local parameters was constrained (at 1 mm and 0.01 mm s^{-1}), as we found this generally resulted in better data fits, but we applied weak constraints when we solved the combined normal equation systems because the states affect the other parameters. For Enceladus, we used 500 m for positions and 10 m s^{-1} for velocities. For Titan, we used 5 km for positions and 100 m s^{-1} for velocities. The results for Enceladus did not change significantly when we used the constraints also used for Titan's state. We applied a constraint of 10% to the solar radiation pressure coefficients, 6% to the drag coefficients (for Titan; for most fly-bys drag was not needed and for low-altitude fly-bys, the drag coefficients have small adjustments of the order of 0.3×10^{-4} from their nominal value of 2.4), 1 mm s^{-1} for velocity adjustments (Enceladus), 0.001 for the RTG accelerations in the xyz directions in the spacecraft frame (for a nominal value of 1; on average they were adjusted at 2 or 3 orders of magnitude below the constraint), and 1 mHz for Doppler three-way biases. All these parameters had only very small adjustments, which did not influence the gravity solutions. All other parameters, such as the gravity field, GM and Love number, were unconstrained.

As stated above, we repeated this process many times, starting with knowledge of only the GM of the fly-by body (8,978 km^3 s^{-2} for Titan and 7.21044 km^3 s^{-2} for Enceladus; all other gravity terms were set to zero), initially estimating only a degree and order 2 field, and gradually increasing the number of spherical harmonic coefficients (for Titan; for Enceladus, we included J_3 only after several iterations). We considered that these global iterations had converged when the residuals fitted close to the noise level (a few millihertz (mHz)) and did not change significantly between iterations (<1%). The data fits did not change much with each increase in expansion (Supplementary Fig. 3), so regardless of changes in fit, we decided to run ten global iterations for each model expansion. Convergence generally was reached well before that. Supplementary Fig. 3 indicates that for several fly-bys, the fit hardly improved. We noticed that in those cases the local parameters

(most notably, Cassini's initial state) showed large adjustments without knowledge of the gravity field (only *GM*) and much smaller adjustments after determination of the gravity field.

When using VCE in our gravity determination, each fly-by was treated as a separate statistical set. VCE determines scale factors for each set with the goal of balancing the formal error statistics with the observed statistics (variations of residuals from cyclically randomizing the statistical sets[40]), and it calibrates the covariance. We show the VCE factors and resulting effective data weights in Supplementary Table 2. Factors larger than 1 mean that the data were upweighted. Because we fitted better than our initial data weight for all fly-bys, all fly-bys were upweighted, some more than others. Note that we did not change the data weights in the determination of the local parameters, but always used 28 mHz. We used only one data type (Doppler), so that the data weight did not affect the values of the local parameters (the weights then affected only the formal errors of the local parameters for each arc, before combining them into one larger system).

We determined k_2 during various expansions of the gravity field model to test the stability of the parameter estimation. We based our final result on the values obtained with a series of degree and order 5 fields. We determined our k_2 value as the uniformly weighted average of k_2 values estimated from these global iterations. The presented uncertainty is the standard deviation of these values around the mean. The set of k_2 values from the degree and order 5 fields were either estimated with the data weighted uniformly at 28 mHz or with the data weighted with the aforementioned VCE factors. Note that, in general, the results from uniformly weighted data produce slightly higher k_2 values than those with the VCE factors.

We show Enceladus's gravity and its associated errors expressed as radial accelerations in Supplementary Fig. 2, including the ground tracks for the fly-bys. The anomalies that are visible are related to ground track coverage; their location was largely determined by the resulting $C_{2,1}$, $S_{2,1}$ and $S_{2,2}$ coefficients. The sign for J_3 resulted in a negative anomaly over the south pole of Enceladus, as found in earlier work[20].

Modelling the tidal effects

The tidal potential U_t can be expressed as[21]

$$U_t = \frac{GM_s}{r_s^3} r^2 P_{2,0}(\cos\psi), \tag{1}$$

where GM_s is Saturn's *GM* (the disturbing body), r_s is the distance to Saturn, r the distance to the computation point, ψ is the angle between the computation point and the centre of Saturn and $P_{2,0}(\cos\psi)$ is the unnormalized degree 2 Legendre function

$$P_{2,0}(\cos\psi) = \frac{1}{2}\left(3\cos^2\psi - 1\right). \tag{2}$$

A general expression for the tidal potential can be obtained by using the addition theorem for Legendre functions

$$P_{n,0}(\cos\psi) = \frac{1}{2n+1}\sum_{m=-n}^{m=n} \bar{Y}_{n,m}(\phi',\lambda')\,\bar{Y}_{n,m}(\phi,\lambda), \tag{3}$$

where n and m are the degree and order, respectively, (ϕ',λ') and (ϕ,λ) are coordinate pairs and ψ is the angle between them. The function $\bar{Y}_{n,m}(\phi,\lambda)$ is defined as

$$\bar{Y}_{n,m}(\phi,\lambda) = \bar{P}_{n,|m|}(\sin\phi)\begin{cases}\cos m\lambda, & m \geq 0,\\ \sin|m|\lambda, & m < 0.\end{cases} \tag{4}$$

The planet's response is equal to the Love number times the tidal potential. Application of the addition theorem in equation (1) (generalizing to all degrees n instead of limiting to degree 2) results in expressions for time-varying changes $\Delta\bar{C}_{n,m}$ and $\Delta\bar{S}_{n,m}$

$$\Delta\bar{C}_{n,m} - \mathrm{i}\Delta\bar{S}_{n,m} = \frac{k_{n,m}}{2n+1}\frac{GM_s}{GM_t}\left(\frac{R_t}{r_s}\right)^{n+1}\bar{P}_{n,m}(\sin\Phi_s)\,\mathrm{e}^{-\mathrm{i}m\lambda_s}, \tag{5}$$

where GM_t is Titan's *GM*, R_t is its radius (2,575 km), $\Delta\bar{C}_{n,m}$ and $\Delta\bar{S}_{n,m}$ are changes to the normalized gravity field coefficients, (λ_s, Φ_s) are the coordinates of Saturn with respect to Titan in Titan's body-fixed frame, and $k_{n,m}$ are Love numbers, now per degree and order. The ratio of radii relates to the attenuation with distance. These coordinates, together with r_s, which describes the distance between Saturn and Titan, vary with time, resulting in time-varying coefficients. This is the general expression as used by the International Earth Rotation and Reference Systems Service (IERS)[29,30]. There is no dependency on order for spherically symmetric planets, and the Love number per degree is simply k_n.

Instead of using changes in the degree 2 gravity coefficients (limiting ourselves now to only degree 2), a direct expression of the tidal potential can also be used

$$U_t = \frac{k_2}{2}\frac{GM_s}{r_s^3}\frac{R_t^5}{r^3}\left(3(\hat{\mathbf{r}}_s\cdot\hat{\mathbf{r}})^2 - 1\right), \tag{6}$$

where $\hat{\mathbf{r}}_s$ is the unit vector between the centres of Titan and Saturn, and $\hat{\mathbf{r}}$ is the unit vector from Titan's centre to the position where the potential is calculated. This expression can be obtained from equation (1) through the definition of the in-product and the angle between two vectors. Both expressions are equivalent, and both implementations are possible with our analysis software. We obtain the same k_2 from them.

The tidal potential can be expressed differently when certain assumptions about Titan's orbit are made. Titan's orbit has a small inclination and eccentricity. Under these assumptions, the potential can be expressed in terms of Titan's eccentricity e and mean anomaly M, and it follows readily that equation (5) includes a static part and a periodic part[12]. This results in expressions for changes in the degree 2 coefficients $C_{2,0}$, $C_{2,2}$ and $S_{2,2}$

$$\Delta C_{2,0} = \Delta C_{2,0}^{\mathrm{static}} + \frac{1}{2}k_2 q_t e\cos M, \tag{7}$$

$$\Delta C_{2,2} = \Delta C_{2,2}^{\mathrm{static}} - \frac{1}{4}k_2 q_t e\cos M, \tag{8}$$

$$\Delta S_{2,2} = \Delta S_{2,2}^{\mathrm{static}} - \frac{1}{3}k_2 q_t e\sin M, \tag{9}$$

where q_t is defined as

$$q_t = -3\frac{GM_s}{GM_t}\left(\frac{R_t}{a}\right)^3, \tag{10}$$

with a the (constant) semimajor axis of Titan's orbit. In this case, the coefficients are unnormalized. Such expressions are convenient because they allow for the separation of the static and periodic effects: one can estimate k_2 from only the periodic contributions to the degree 2 terms, which is how it was done in previous analyses[3,6]. It should then also be made clear that the contribution of the permanent tide is accounted for in the static gravity field coefficients (J_2, $C_{2,2}$ and $S_{2,2}$). Such coefficients are called 'zero tide'[30]. If the contribution of the permanent tide is not included, the degree 2 coefficients are called 'conventional tide free'[30].

It is not readily clear from equation (5) that there is a permanent tide contribution. It is explicit only for $\Delta\bar{C}_{2,0}$ because $\bar{P}_{2,0}$ has a constant term (equation (2)). However, by using Taylor expansions for small

angles Φ_s and λ_s, it will be clear that there are also constant terms for the order 2 coefficients $\Delta\bar{C}_{2,2}$ and $\Delta\bar{S}_{2,2}$.

Separating the permanent and periodic contributions and using only the periodic terms to estimate k_2 result in lower correlations between k_2 and the degree 2 gravity terms. With the permanent contribution included, the correlation between $\bar{C}_{2,0}$ and k_2 is 0.96 and that between $\bar{C}_{2,2}$ and k_2 is −0.99; they reduce to 0.36 and 0.13 when the permanent contribution is removed. Our analysis shows that this also results in lower formal errors but without changing the estimated value itself. Without k_2 estimation, our solution also resulted in a lower error at degree 2 (Fig. 2). Our analysis mostly used equation (6) to account for the tides. From this expression it is not readily clear that there is a constant for certain degree 2 terms; there is a constant term in the potential but it still depends on r_s, which varies with time. The same assumptions about Titan's orbit could be made to isolate a constant contribution to the tidal potential of equation (6), but we used the expression as is. Our formal error at degree 2 is, thus, higher (Fig. 2), but this did not affect the value of the estimated coefficients.

Although some assumptions were made to obtain the expressions in equations (7)–(9), these assumptions are very reasonable. Differences in the time variations of the degree 2 terms between the two sets of expressions (equation (5) and equations (7)–(9)) are small (Supplementary Fig. 8). Note that the simplified potential does not have time variations for the degree 2, order 1 terms, whereas those from equation (5) do. They are, however, much smaller than those for the other terms (Supplementary Fig. 9).

Estimating k_2

The general linearized observation equation that relates changes in data residuals $\Delta\boldsymbol{\rho}$ to changes in parameters $\Delta\mathbf{p}$ is given as

$$\Delta\boldsymbol{\rho} = A\Delta\mathbf{p}, \tag{11}$$

where A is the partial derivative matrix that relates the two. Partial derivatives are obtained through the numerical integration of the variational equations[38,39].

The Love number k_2 is estimated from tracking data through its effect on the gravity field of the central body. As explained above, the tides raise a potential and, thus, a force; this potential can be expressed directly as in equation (6), or it can be related to time variations in the degree 2 gravity coefficients as in equation (5).

When using the time-variable effect of k_2 on the degree 2 terms (compare with equation (5)), the generation of the k_2 partials requires a chaining of the effects of degree 2 coefficients (denoted $v_{n,m}$ to indicate both $C_{n,m}$ and $S_{n,m}$ coefficients, where $m < 0$ denotes the $S_{n,m}$ terms and $m \geq 0$ denotes the $C_{n,m}$ terms) with partials of those coefficients with respect to k_2. Such partials $\partial v_{n,m}/\partial k_2$ can be obtained, either from equation (5) for the general case or from equations (7)–(9) for the approximated case.

In previous work[6], the partials of measurements with respect to k_2 are expressed through their effects on the degree 2 coefficients as follows:

$$\frac{\partial\rho}{\partial k_2} = \sum_{m=-2}^{m=2}\left[\frac{\partial\rho}{\partial v_{2,m}}\frac{\partial v_{2,m}}{\partial k_2}\right]. \tag{12}$$

The partials $\partial\rho/\partial v_{2,m}$ are obtained as output from the orbit determination (and, thus, after numerical integration of the variational equations), and they are then multiplied afterwards with the respective k_2 partials, evaluated at the time of the observation, to obtain the total partial for k_2. However, the partials $\partial v_{2,m}/\partial k_2$ are time-dependent but in this way this time dependence is not accounted for in the integration of the variational equations.

The variational equations for estimating the model parameters $\mathbf{p}$ are obtained from the equations of motion that relate the spacecraft state $\mathbf{x}$ (both position and velocity), the parameters and forces $\mathbf{f}$ acting on the spacecraft through

$$\frac{\mathrm{d}}{\mathrm{d}t}\mathbf{x} = \mathbf{f}(t,\mathbf{x},\mathbf{p}) = \dot{\mathbf{x}}(t,\mathbf{x},\mathbf{p}). \tag{13}$$

The variational equations can then be derived as

$$\frac{\mathrm{d}}{\mathrm{d}t}\frac{\partial\mathbf{x}}{\partial\mathbf{p}} = \frac{\partial\dot{\mathbf{x}}}{\partial\mathbf{x}}\frac{\partial\mathbf{x}}{\partial\mathbf{p}} + \frac{\partial\dot{\mathbf{x}}}{\partial\mathbf{p}}. \tag{14}$$

For clarity, using only k_2 for $\mathbf{p}$, this would read

$$\frac{\mathrm{d}}{\mathrm{d}t}\frac{\partial\mathbf{x}}{\partial k_2} = \frac{\partial\dot{\mathbf{x}}}{\partial\mathbf{x}}\frac{\partial\mathbf{x}}{\partial k_2} + \frac{\partial\dot{\mathbf{x}}}{\partial k_2}. \tag{15}$$

The partial $\partial\dot{\mathbf{x}}/\partial k_2$ is obtained by chaining it with $\partial v_{2,m}/\partial k_2$. To illustrate, if we limit ourselves to the effect of k_2 on $\bar{C}_{2,2}$ (to avoid summation over all five degree 2 terms), this partial has to be chained in the following way:

$$\frac{\partial\dot{\mathbf{x}}}{\partial k_2} = \frac{\partial\dot{\mathbf{x}}}{\partial\bar{C}_{2,2}}\frac{\partial\bar{C}_{2,2}}{\partial k_2}. \tag{16}$$

Here, normalized coefficients are used because the coefficients in the processing software are normalized. For the variational equation, this results in

$$\frac{\mathrm{d}}{\mathrm{d}t}\frac{\partial\mathbf{x}}{\partial k_2} = \frac{\partial\dot{\mathbf{x}}}{\partial\mathbf{x}}\frac{\partial\mathbf{x}}{\partial k_2} + \frac{\partial\dot{\mathbf{x}}}{\partial\bar{C}_{2,2}}\frac{\partial\bar{C}_{2,2}}{\partial k_2}. \tag{17}$$

The partial $\partial\bar{C}_{2,2}/\partial k_2$ varies with time and, thus, has to be accounted for directly during the numerical integration of the variational equations. When using equation (12), this is not the case. Only $\partial\rho/\partial v_{2,m}$ is obtained through the variational equations.

This results in different partials. We show the difference between k_2 partials obtained through the variational equations and those without (that is, following equation (12)) in Supplementary Fig. 10 for fly-by T022. We call the latter partials 'non-variational', with the understanding that the partial $\partial\rho/\partial v_{n,m}$ is, in fact, a result obtained through the variational equations; it is just that it is then multiplied with the $\partial v_{n,m}/\partial k_2$ partial. For this example, we used the formulation from equation (5) to ensure that we have the same $\partial v_{n,m}/\partial k_2$ values (this, thus, excludes the factor of 2 error in the $S_{2,2}$ term; see discussion below). It is clear that these k_2 partials are different, especially after the closest approach. This, thus, has an effect on the estimate for k_2 because the partials in the matrix A in equation (11) will be different.

We tested whether, indeed, changes in k_2 predicted changes in the data residuals by using equation (11). We propagated an orbit for a span of time using a value k_2^a. We computed tracking data residuals for this value. We then perturbed k_2^a into $k_2^b = k_2^a + \Delta k_2$ and computed new residuals. We then used equation (11) to test the partial. If all is correct, then the difference in residuals should be matched by the partial times the change in k_2.

We show residual changes and predicted changes in Supplementary Fig. 11. Instead of using a Cassini fly-by, we used an example from the processing of Gravity Recovery and Interior Laboratory (GRAIL) intersatellite Ka-band range-rate data, simply because a satellite in orbit around a body is more sensitive to tidal effects. The principle as well as the result is the same, however, as if we were to use Cassini data: small changes in parameters should result in changes in residuals as predicted by the partials in the linear regime. We perturbed k_2 by 0.02 for a nominal value of 0.024, which is a relatively large change. Supplementary Fig. 11 shows that the changes in residuals match when the partials were computed with the variational partials (showing that

the linearization holds despite the relatively large change in k_2), but the differences are large when they were computed with the non-variational partials. This clearly shows that the non-variational partials do not satisfy the basic observation equation (11).

In addition, to illustrate how this affects the analysis of Cassini data, we show the difference in predicted residuals between those from the variational partials and those from the non-variational partials for fly-by T022 in Supplementary Fig. 12. For this case, we used a Δk_2 of 0.25. This shows that the difference in partials as shown in Supplementary Fig. 10 results in residual differences that increase after the closest approach. This indicates the extent to which the observation equation, equation (11), is not satisfied with the non-variational partials.

Finally, we investigated the effect on the estimate of k_2. We focused only on a case where initially $k_2 = 0$, and we did not iterate this. We selected the case $k_2 = 0$ to avoid differences in the tidal model, which would lead to differences in the orbits and partials. The results from this test were, therefore, different from our final solution of k_2. Here we want to demonstrate only the influence of different partials on the estimation of k_2. We, thus, made sure that the base ingredients for the tests that follow hereafter are the same for each case.

We generated partial derivatives for the entire Cassini dataset from our standard processing. We then used either the direct partials or we replaced them with partials computed from equation (12). For the latter, we can either use the IERS expressions or the approximated expressions[12] to compute $\partial v_{2,m}/\partial k_2$. Also note that in the earlier results for Titan[6], there is a mistake in the expression for $S_{2,2}$. The periodic term for $S_{2,2}$ has a factor of 1/6, which should be 1/3; see equation (9)[12]. We also tested the effect of this. Related to this, we generated partials from our standard processing but without the constant contributions to the degree 2 terms (while still using the fully variational approach). With this, we corrupted the $S_{2,2}$ contribution with a factor of a half to test this effect. We show results for k_2 for various cases in Supplementary Table 3.

The results indicate that the choice of partials has a large influence: not using the full variational approach but with the same IERS expressions from equation (5), listed as the case 'non-variational partial; IERS', already changed the k_2 value. Results with the non-variational partials are in general higher than the result with the variational partial. The range of the k_2 values that we obtained is, however, within the error bars of our own estimate. Yet when we include the mistake in the $S_{2,2}$ partial, k_2 increased further and became much closer to that reported before[3,6]. Thus, we can replicate the earlier results by using the approximated tidal potential together with the mismatch in the $S_{2,2}$ term and the non-variational partials. Leaving out the permanent contributions to the degree 2 terms does not significantly affect the k_2 value when using the variational partials. The error in the $S_{2,2}$ term does increase the k_2 value but not as much as when the non-variational partials are used. Although the partial differences in Supplementary Fig. 10 and the residual differences in Supplementary Fig. 12 may seem small, this inversion test shows that there is a strong effect on the estimate of k_2.

That the $S_{2,2}$ partial has such a big influence was somewhat surprising, as it was expected that the estimate of k_2 would mostly be driven by $C_{2,0}$ and $C_{2,2}$ variations. As mentioned above, when we corrupted the $S_{2,2}$ contribution with a factor of 2 in our own processing using the fully variational partials, we did not see such a large increase in the estimated k_2 value. However, when correcting for the permanent contributions to k_2 by the degree 2 terms, the size of the time-varying $S_{2,2}$ coefficient became comparable to the contributions of $C_{2,0}$ and $C_{2,2}$. This means that the $S_{2,2}$ term has a larger effect than when the permanent contribution to k_2 is not separated. This explains the relatively large contribution of the $S_{2,2}$ term in the previous analysis.

The degree 2, order 1 terms, which are assumed to be zero in the approximated approach[12], indeed do not contribute much to the estimate of k_2, which we tested by excluding them.

Interior modelling

We modelled the interior of Enceladus and Titan using homogeneous layers. For Enceladus, we assumed a three-layer model with a core, ocean and crust. We acknowledge that variations in Enceladus's ice shell thickness can have an influence[41], but we are not considering Enceladus's tidal response in this work. We fixed the density of the ocean and crust because we have only the moment of inertia factor to constrain the radial density profile, and the density contrast between ocean and icy crust is probably difficult to resolve from the constraints. The ocean density was set to 1,020 kg m^{-3} and that of the (icy) crust to 925 kg m^{-3}; these are in the range that we used for Titan (see below) and follow earlier work[17]. The core density was then computed to match the bulk density of 1,611 kg m^{-3}, which was obtained from Enceladus's *GM* (Supplementary Table 1) and its radius of 252 km. For a three-layer model, the core density ρ_{core} depends then on the core radius and ocean thickness:

$$\rho_{\mathrm{core}} = \frac{\rho_{\mathrm{bulk}} R_{\mathrm{e}}^3 - \rho_{\mathrm{ocean}} \left(r_{\mathrm{ocean}}^3 - r_{\mathrm{core}}^3\right) - \rho_{\mathrm{ice}} \left(R_{\mathrm{e}}^3 - r_{\mathrm{ocean}}^3\right)}{r_{\mathrm{core}}^3}, \qquad (18)$$

where R_{e} is Enceladus's radius, ρ_{bulk} is the bulk density, and the other densities and radii refer to the other layers.

We used an MCMC analysis, using the open source 'emcee' software[32], to explore Enceladus's structure by varying the core radius and ocean thickness to match the bulk density (with a 2% error) and polar moment of inertia factor ($C/(MR^2) = 0.345 \pm 0.01$). We assumed an ocean thickness of at least 5 km and also ensured that the icy crust was at least 10 km thick. We could have varied more parameters but doing so does not change that the solutions were mostly sensitive only to the core radius and density. We ran 100,000 models using 40 chains and found that we could resolve only the core parameters. We show histograms for the core radius and core density in Supplementary Fig. 13. We found a core radius of 201 ± 12 km and a density of 2,202 ± 242 kg m^{-3} from the modes of the distributions. This is a slightly larger core with a lower density than earlier analysis[42] but still consistent with it considering the errors that we obtained.

We modelled Titan's structure in much the same way with four layers: a core, high-pressure ice, an ocean and a crust. We varied the core radius and density, ocean thickness and density, the viscosity of the high-pressure ice and crust, and the core's unrelaxed rigidity. Because we included Titan's k_2 as a measurement, we had to include rigidities, viscosities and bulk moduli as well. We used values from earlier work[17] for the fixed parameters. We fixed the density of the high-pressure ice to 1,340 kg m^{-3} and that of the icy crust to 925 kg m^{-3} following earlier work[14,17]. We also set the thickness of the high-pressure ice to 150 km, following earlier work[14] and considering the lack of sensitivity. Our results did not change significantly when we varied the thickness of this layer. To compute Titan's Love number, we fixed the bulk moduli for all layers: 200 GPa for the core, 20 GPa for the high-pressure ice, 2.5 GPa for the ocean and 10 GPa for the icy crust[17]. We fixed unrelaxed rigidities (shear moduli) for all but the core: 10 GPa for the high-pressure ice, 0 for the ocean and 3 GPa for the icy crust[17]. A recent analysis[31] found different shear and bulk moduli for the core than an earlier analysis[17]. We found that changing these parameters had only a very small effect on k_2, as was also found by the earlier analysis. We used a Maxwell rheology for Titan but obtained the same results with an Andrade rheology.

We list the values and ranges for those parameters that were varied in Supplementary Table 4. For Titan, we assumed an ocean thickness of at least 50 km and an icy crust thickness of also at least 50 km. Density inversions were not allowed. Thus, the ocean density was always between 925 and 1,340 kg m^{-3} (we did not limit it to be at least 1,000 kg m^{-3} and this did not affect the results). For this MCMC analysis, we computed 500,000 models with 40 chains to match the bulk density (with again a 2% error), the moment of inertia ($C/(MR^2) = 0.348 \pm 0.03$) and the Love number ($k_2 = 0.375 \pm 0.06$).

We modelled Titan's tidal response using the open source software TidalPy[43]. We used a Maxwell rheology. When we used an Andrade rheology, we used parameter values $\alpha = 0.3$ and $\zeta = 1.0$. We did not explore variations of these parameters.

Data availability

Cassini radio tracking data and ancillary information can be found at the Planetary Data System's Atmospheres node (https://pds-atmospheres.nmsu.edu/data_and_services/atmospheres_data/Cassini/inst-rss.html). Results from our analysis such as the gravity field models and output from our MCMC modelling are available via NASA's Planetary Geodesy Data Archive at https://pgda.gsfc.nasa.gov/products/91 or https://doi.org/10.60903/gsfcpgda-titank2.

Code availability

We used the open source software TidalPy to analyse Titan's Love number (https://doi.org/10.5281/zenodo.7017474 (ref. 43)) and the emcee open source software[32] for our MCMC analysis (https://emcee.readthedocs.io/en/stable/). We also used the PlanetProfile software[44] (https://github.com/vancesteven/PlanetProfile) to compute the self-consistent interior models for Titan used in our modelling. The input data for the MCMC analysis are the results presented in this work; additional input parameters for TidalPy are discussed in the text and listed in Supplementary Table 4. We also used the Python package corner[45] for the distribution plot in Supplementary Information. We cannot provide the software used for the analysis of the Cassini tracking data, but the methods have long been established and are described in detail in Methods. All figures (apart from the distribution plot in Supplementary Fig. 5) were drawn with the free software GMT (https://www.generic-mapping-tools.org/)[46].

References

1. Iess, L. et al. Gravity field, shape, and moment of inertia of Titan. *Science* **327**, 1367–1369 (2010).
2. Tortora, P. et al. Rhea gravity field and interior modeling from Cassini data analysis. *Icarus* **264**, 264–273 (2016).
3. Durante, D., Hemingway, D. J., Racioppa, P., Iess, L. & Stevenson, D. J. Titan's gravity field and interior structure after Cassini. *Icarus* **326**, 123–132 (2019).
4. Zannoni, M., Hemingway, D., Gomez Casajus, L. & Tortora, P. The gravity field and interior structure of Dione. *Icarus* **345**, 113713 (2020).
5. Iess, L. et al. Measurement and implications of Saturn's gravity field and ring mass. *Science* **364**, aat2965 (2019).
6. Iess, L. et al. The tides of Titan. *Science* **337**, 457–459 (2012).
7. Lunine, J. I. & Stevenson, D. J. Clathrate and ammonia hydrates at high pressure: application to the origin of methane on Titan. *Icarus* **70**, 61–77 (1987).
8. Grasset, O. & Sotin, C. The cooling rate of a liquid shell in Titan's interior. *Icarus* **123**, 101–112 (1996).
9. Grasset, O., Sotin, C. & Deschamps, F. On the internal structure and dynamics of Titan. *Planet. Space Sci.* **48**, 617–636 (2000).
10. Sohl, F., Hussmann, H., Schwentker, B., Spohn, T. & Lorenz, R. D. Interior structure models and tidal Love numbers of Titan. *J. Geophys. Res. Planets* **108**, 5130 (2003).
11. Rappaport, N., Bertotti, B., Giampieri, G. & Anderson, J. D. Doppler measurements of the quadrupole moments of Titan. *Icarus* **126**, 313–323 (1997).
12. Rappaport, N. J. et al. Can Cassini detect a subsurface ocean in Titan from gravity measurements? *Icarus* **194**, 711–720 (2008).
13. Sohl, F. et al. Structural and tidal models of Titan and inferences on cryovolcanism. *J. Geophys. Res. Planets* **119**, 1013–1036 (2014).
14. Sotin, C., Kalousová, K. & Tobie, G. Titan's interior structure and dynamics after the Cassini–Huygens mission. *Annu. Rev. Earth Planet. Sci.* **49**, 579–607 (2021).
15. Stiles, B. W. et al. Determining Titan's spin state from Cassini RADAR images. *Astron. J.* **135**, 1669–1680 (2008).
16. Zebker, H. A. et al. Size and shape of Saturn's moon Titan. *Science* **324**, 921–923 (2009).
17. Mitri, G. et al. Shape, topography, gravity anomalies and tidal deformation of Titan. *Icarus* **236**, 169–177 (2014).
18. Baland, R.-M., Tobie, G., Lefèvre, A. & Van Hoolst, T. Titan's internal structure inferred from its gravity field, shape, and rotation state. *Icarus* **237**, 29–41 (2014).
19. Beuthe, M. Tidal Love numbers of membrane worlds: Europa, Titan, and co. *Icarus* **258**, 239–266 (2015).
20. Iess, L. et al. The gravity field and interior structure of Enceladus. *Science* **344**, 78–80 (2014).
21. Murray, C. & Dermott, S. *Solar System Dynamics* (Cambridge Univ. Press, 1999).
22. Meriggiola, R., Iess, L., Stiles, B. W., Lunine, J. I. & Mitri, G. The rotational dynamics of Titan from Cassini RADAR images. *Icarus* **275**, 183–192 (2016).
23. Fortes, A. D. Titan's internal structure and the evolutionary consequences. *Planet. Space Sci.* **60**, 10–17 (2012).
24. Gao, P. & Stevenson, D. J. Nonhydrostatic effects and the determination of icy satellites' moment of inertia. *Icarus* **226**, 1185–1191 (2013).
25. Coyette, A., Baland, R.-M. & Van Hoolst, T. Variations in rotation rate and polar motion of a non-hydrostatic Titan. *Icarus* **307**, 83–105 (2018).
26. Zharkov, V. N., Leontjev, V. V. & Kozenko, V. A. Models, figures, and gravitational moments of the Galilean satellites of Jupiter and icy satellites of Saturn. *Icarus* **61**, 92–100 (1985).
27. Asmar, S. W., Armstrong, J. W., Iess, L. & Tortora, P. Spacecraft Doppler tracking: noise budget and accuracy achievable in precision radio science observations. *Radio Sci.* **40**, RS2001 (2005).
28. Ermakov, A. I., Park, R. S. & Bills, B. G. Power laws of topography and gravity spectra of the Solar System bodies. *J. Geophys. Res. Planets* **123**, 2038–2064 (2018).
29. Eanes, R., Schutz, B. & Tapley, B. Earth and ocean tide effects on Lageos and Starlette. In *Proc. 9th International Symposium on Earth Tides* (ed. Kuo, J. T.) 239–249 (E. Schweizerbart, 1983).
30. McCarthy, D. D. & Petit, G. *IERS Conventions (2003)* Technical Note 32 (IERS, 2004).
31. Vance, S. D. et al. Geophysical investigations of habitability in ice-covered ocean worlds. *J. Geophys. Res. Planets* **123**, 180–205 (2018).
32. Foreman-Mackey, D., Hogg, D. W., Lang, D. & Goodman, J. emcee: The MCMC hammer. *Publ. Astron. Soc. Pac.* **125**, 306 (2013).
33. Pavlis, D. E. & Nicholas, J. B. GEODYN II system description (vols. 1–5). Contractor report, (SGT Inc., 2017); https://earth.gsfc.nasa.gov/geo/data/geodyn-documentation
34. Bertotti, B., Iess, L. & Tortora, P. A test of general relativity using radio links with the Cassini spacecraft. *Nature* **425**, 374–376 (2003).
35. Archinal, B. A. et al. Report of the IAU Working Group on Cartographic Coordinates and Rotational Elements: 2015. *Celest. Mech. Dyn. Astron.* **130**, 22 (2018).
36. Bellerose, J., Roth, D. & Criddle, K. in *Space Operations: Inspiring Humankind's Future* (eds Pasquier, H. et al.) 575–588 (Springer, 2019); https://arc.aiaa.org/doi/10.2514/6.2018-2646
37. Barbaglio, F., Armstrong, J. W. & Iess, L. Precise Doppler measurements for navigation and planetary geodesy using low gain antennas: test results from Cassini. In *Proc. 23rd International Symposium on Space Flight Dynamics* (German Aerospace Center, 2012); https://issfd.org/ISSFD_2012/ISSFD23_OD1_4.pdf
38. Montenbruck, O. & Gill, E. *Satellite Orbits* (Springer-Verlag, 2000).
39. Tapley, B. D., Schutz, B. E. & Born, G. H. *Statistical Orbit Determination* (Elsevier, 2004).

40. Kusche, J. Noise variance estimation and optimal weight determination for GOCE gravity recovery. *Adv. Geosci.* **1**, 81–85 (2003).
41. Běhounková, M., Souček, O., Hron, J. & Čadek, O. Plume activity and tidal deformation on Enceladus influenced by faults and variable ice shell thickness. *Astrobiology* **17**, 941–954 (2017).
42. Hemingway, D. J. & Mittal, T. Enceladus's ice shell structure as a window on internal heat production. *Icarus* **332**, 111–131 (2019).
43. Renaud, J. P. TidalPy (0.4.1). *Zenodo* https://doi.org/10.5281/zenodo.7017474 (2023).
44. Styczinski, M. J., Vance, S. D. & Melwani Daswani, M. Planetprofile: self-consistent interior structure modeling for ocean worlds and rocky dwarf planets in Python. *Earth Space Sci.* **10**, e2022EA002748 (2023).
45. Foreman-Mackey, D. corner.py: scatterplot matrices in Python. *J. Open Source Softw.* **1**, 24 (2016).
46. Wessel, P., Smith, W. H. F., Scharroo, R., Luis, J. & Wobbe, F. Generic Mapping Tools: improved version released. *Eos Trans. Am. Geophys. Union* **94**, 409–410 (2013).
47. Kaula, W. M. *Theory of Satellite Geodesy, Applications of Satellites to Geodesy* (Blaisdell Publishing Company, 1966).

Acknowledgements

This work was funded by NASA's Cassini Data Analysis Program (S.G., B.v.N. and E.M.). We thank T. Sabaka (NASA/GSFC), S. Bertone (NASA/GSFC, University of Maryland, Baltimore County, and CRESST II), W. Henning and J. Renaud (NASA/GSFC, University of Maryland and CRESST II), G. Cascioli (NASA/GSFC and University of Maryland, Baltimore County), and D. Durante and L. Iess (Sapienza University of Rome, Italy) for discussions.

Author contributions

S.G. and E.M. conceived and designed the study. S.G., B.v.N. and A.M. analysed the Cassini tracking data. E.M. supported the analysis of the Cassini tracking data. W.v.d.W. provided theoretical support. All authors contributed to the discussion and interpretation of the results. S.G. wrote the first draft of the paper. All authors contributed to subsequent drafts.

Competing interests

The authors declare no competing interests.

Additional information

Supplementary information The online version contains supplementary material available at https://doi.org/10.1038/s41550-024-02253-4.

Correspondence and requests for materials should be addressed to Sander Goossens.

Peer review information *Nature Astronomy* thanks Sebastien Le Maistre, Marzia Parisi and the other, anonymous, reviewer(s) for their contribution to the peer review of this work.